Materials Today Bio 23 (2023) 100800

Contents lists available at ScienceDirect

Materials Today Bio

journal homepage: www.journals.elsevier.com/materials-today-bio

Lineage-specific multifunctional double-layer scaffold accelerates the integrated regeneration of cartilage and subchondral bone

Chunhui Ma [a], Tao Wang [a], Xinmeng Jin [a], Wanglin Zhang [b,**], Qi Lv [c,*]

[a] Department of Orthopedic Surgery, Shanghai General Hospital, Shanghai Jiao Tong University, Shanghai, 200080, China
[b] Department of Orthopaedics, Shanghai Children's Medical Center, Shanghai Jiaotong University School of Medicine, Shanghai, China
[c] Department of Medical Imaging, Tongji Hospital, School of Medicine, Tongji University, Shanghai, 200065, China

ARTICLE INFO

Keywords:
Hyaluronic acid
Starved BMSCs-EVs
Haematoma
Osteochondral defects
Lineage-specific scaffold

ABSTRACT

Repairing cartilage/subchondral bone defects that involve subchondral bone is a major challenge in clinical practice. Overall, the integrated repair of the structure and function of the osteochondral (OC) unit is very important. Some studies have demonstrated that the differentiation of cartilage is significantly enhanced by reducing the intake of nutrients such as lipids. This study demonstrates that using starvation can effectively optimize the therapeutic effect of bone marrow mesenchymal stem cells (BMSCs)-derived extracellular vesicles (EVs). A hyaluronic acid (HA)-based hydrogel containing starved BMSCs-EVs displayed continuous release for more than 3 weeks and significantly promoted the proliferation and biosynthesis of chondrocytes around the defect regulated by the forkhead-box class O (FOXO) pathway. When combined with vascular inhibitors, the hydrogel inhibited cartilage hypertrophy and facilitated the regeneration of hyaline cartilage. A porous methacrylate gelatine (GelMA)-based hydrogel containing calcium salt loaded with thrombin rapidly promoted haematoma formation upon contact with the bone marrow cavity to quickly block the pores and prevent the blood vessels in the bone marrow cavity from invading the cartilage layer. Furthermore, the haematoma could be used as nutrients to accelerate bone survival. The in vivo experiments demonstrated that the multifunctional lineage-specific hydrogel promoted the integrated regeneration of cartilage/subchondral bone. Thus, this hydrogel may represent a new strategy for osteochondral regeneration and repair.

1. Introduction

Osteochondral defects typically involve articular cartilage and deep subchondral bone [1]. Due to increasingly serious medical needs, various surgical treatments have been performed to repair OC defects, including autologous chondrocyte implantation, microfracture, inlay and autotransplantation [2]. These traditional therapies are typically complex and result in the lack of biomechanical functions in fibrocartilage [3]. The development of tissue engineering materials based on cells, biomaterials and active factors exhibits advantages in repairing OC defects. The tissue repair materials developed in this study are based on natural polymers and mineral matrices with good biocompatibility. Hyaluronic acid and gelatine are both natural extracellular matrices existing in cartilage and bone [4–7]. They are widely used in tissue regeneration due to their good biocompatibility, degradability and rapid regeneration abilities. To further compensate for their deficiencies in OC defect repair, it is necessary to introduce active ingredients to improve biological activity. However, due to the significant differences between chemical composition and biological lineage, the design and application of lineage-specific multifunctional scaffolds are needed (see Scheme 1).

In the lineage-specific regeneration process, the cell source and biological cues are important. Regarding the cell source, although mesenchymal stem cells (MSCs) from the bone marrow exhibit ability to differentiate into multiple different lineages, including cartilage and osteogenic tissue, the formed cartilage often undergoes endochondral osteogenesis (ECO), leading to cartilage tissue repair failure. Therefore, the aim here is to activate the vitality of chondrocytes around cartilage defects to accelerate repair while promoting the osteogenic differentiation of bone marrow mesenchymal stem cells to accelerate subchondral bone repair. Because the slow proliferation of chondrocytes limits

* Corresponding author.
** Corresponding author.
E-mail addresses: drmachunhui@163.com (C. Ma), wtfamily@163.com (T. Wang), jinxinmeng2023@163.com (X. Jin), zhang.wanglin@yahoo.com (W. Zhang), 1500121@tongji.edu.cn (Q. Lv).

https://doi.org/10.1016/j.mtbio.2023.100800
Received 8 May 2023; Received in revised form 4 September 2023; Accepted 14 September 2023
Available online 16 September 2023

repair, suitable biological cues regulating cell function are necessary. Such a microenvironment consists of two basic components: the extracellular matrix (ECM) and the growth factors secreted by cells. As the functional paracrine factor of mesenchymal stem cells (MSCs), extracellular vesicles (EVs) derived from MSCs can transmit genetic and functional information and exhibit comparative advantages over stem cells [8,9]. Furthermore, EVs exhibit lower immunogenicity, better safety and experimental control [10]. EVs have become an attractive alternative to cell therapy in regenerative medicine because they can differentiate into multiple lineages, such as chondrocytes, osteoblasts, or adipocytes [11,12]. The hypoxic microenvironment of cartilage lacks blood vessels and is thus different from the metabolic milieu of bone tissue. Some studies have demonstrated that starvation treatment, compared with normal treatment, reduces chondrocyte apoptosis under starvation conditions [13]. Furthermore, some studies have suggested that cartilage differentiation is significantly enhanced by reducing the intake of nutrients such as lipids [14]. Therefore, hydrogel-loaded starved BMSCs-EVs were developed as an intraarticular delivery platform for accelerating cartilage regeneration. Furthermore, the infiltration of endothelial cells and the formation of vessels could regulate the hypertrophy and vascularization of cartilage during the process of endochondral solidification, which ultimately leads to the formation of granulation tissue and bone tissue to replace hyaline cartilage. Notably, antiangiogenic therapies for cartilage regeneration have already successfully promoted the regeneration of hyaline cartilage [15].

An attractive strategy to prepare lower layer hydrogels that can quickly repair bone is by haematoma formation in situ. During tissue healing, a series of biological events, including haematoma formation, occur, which not only prevents blood loss but also fills defects. As a temporary scaffold for further repair, the haematoma contains various factors that can promote the repair process [16]. The quality of the blood clots (haematomas) impacts subsequent inflammatory regulation, callus formation, and bone remodelling [17,18]. Next, endothelial cells and fibroblasts invade the haematoma and form capillaries and fibrous tissue to establish a more stable microenvironment for subsequent osteogenesis [19,20]. Inspired by the natural coagulation process, bionic scaffold/hydrogel and blood prefabrication strategies have aroused great interest when developing functional bone substitutes. Changes in fracture haematomas can significantly accelerate or damage the whole bone healing process [16]. Blood coagulation during tissue healing can not only prevent blood loss but also act as a scaffold to promote tissue repair and regeneration [21,22].

Based on the above, in this study, functional EVs were prepared by starvation, and a vascular inhibitor (bevacizumab, a silencer of VEGF (sVEGF)) was loaded in HA hydrogels to prepare cartilage-layered hydrogels for cartilage repair. Additionally, a porous GelMA-based hydrogel containing calcium salt and thrombin was prepared to promote the rapid adsorption and coagulation of blood in the marrow cavity [18]. Moreover, calcium-containing hydrogels have been shown to stimulate the proliferation, differentiation and maturation of osteoblasts in vitro [23–25]. The haematoma formed can not only prevent later vascular invasion into the cartilage layer, which makes the cartilage unstable, but also accelerate bone survival. This lineage-specific multifunctional double-layer scaffold provides a new strategy and novel materials for the integrated regeneration of cartilage and subchondral bone.

2. Materials and methods

2.1. Materials

Methacrylated Hyaluroninc acid (MAHA), GelMA (82% degree of substitution) and calcium chloride were purchased from Aladdin. Lithium phenyl-2,4,6-trimethylbenzoylphosphinate (LAP) was purchased from Sigma−Aldrich. Thrombin was purchased from Macklin. Bevacizumab was purchased from MedChemExpress (MCE).

2.2. Extraction and identification of EVs

BMSCs (2×10^5) were cultured in 25T flasks under starvation (serum and glucose deprivation) conditions. EV isolation was performed using ultracentrifugation. Briefly, when the cells reached 80% confluence,

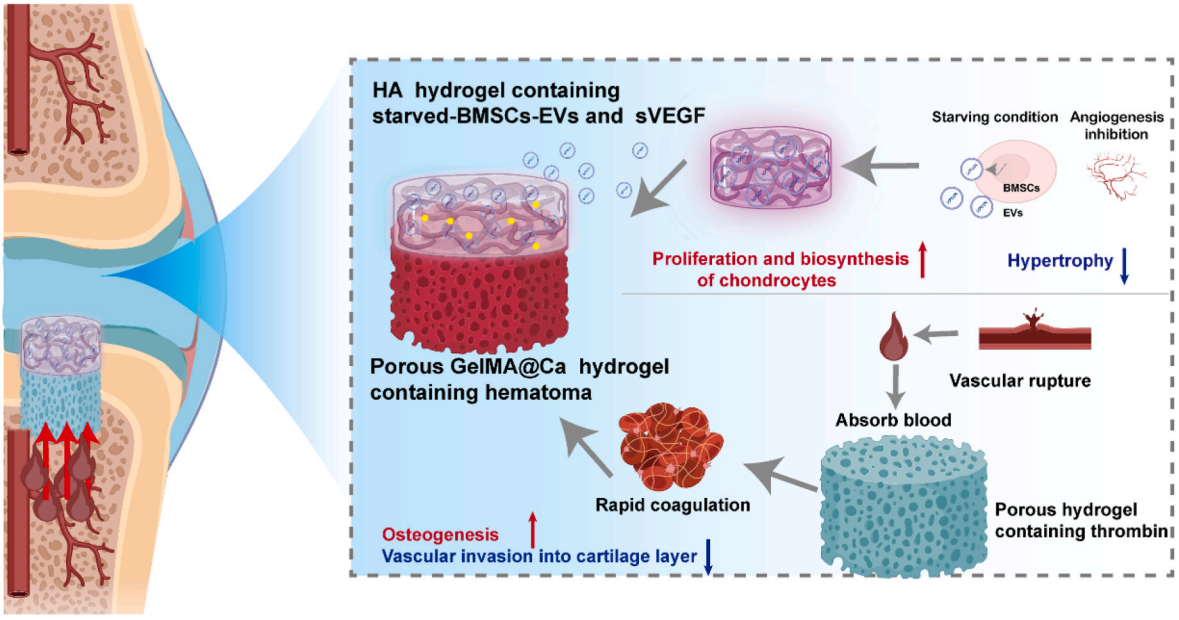

Scheme 1. Lineage-specific multifunctional double-layer scaffolds accelerate the integrated regeneration of cartilage and subchondral bone. The upper layer is composed of an HA-based hydrogel loaded with starved BMSCs-Evs and sVEGF. By releasing starved BMSCs-Evs and sVEGF, the hydrogel can activate the activity of chondrocytes, promote the proliferation and biosynthesis of a small number of chondrocytes in the cartilage defect after in situ implantation, and reduce the cartilage hypertrophy, thus forming stable cartilage. The lower layer is composed of collagen-based hydrogel containing calcium and thrombin. By optimizing the structure of the gel and the content of thrombin, the blood in the bone marrow cavity can be quickly absorbed and solidified to form a haematoma after being implanted into the body to promote bone formation and prevent the blood vessels in the bone marrow cavity from invading the cartilage layer.

cells under normal or starved conditions were washed with PBS, and a-MEM without serum was added to continue culture for 24 h to collect the EVs. The supernatant of the culture medium was collected and centrifuged at 1500 *g* for 10 min to remove cell fragments. The collected supernatant liquid was further centrifuged at 5000 *g* in an Amicon Ultra-15 ultrafiltration tube (Millipore, USA) for 15 min and again at 100000 *g* in a sterile Ultra-ClearTM tube (Beckman Colter, USA) for 90 min to obtain concentrated extracellular vesicles. All processes were conducted at 4 °C. The concentrated EVs were stored at −80 °C for subsequent experiments. The EV concentration was determined by nanoparticle tracking analysis (NTA). The original concentration was diluted to 1×10^{10} for storage and use.

The morphology of starved BMSCs-EVs was observed by transmission electron microscopy (TEM) (JEM 1400, Tokyo, Japan). The particle size distribution was determined by NTA. EV surface markers, including CD81, TSG101, and calnexin, were analysed by Western blot assays. To detect the phagocytosis of starved BMSCs-EVs by BMSCs and chondrocytes, starved BMSCs-EVs labelled with the dye PKH26 at a concentration of 1×10^{10} were cocultured with 5000 cells in 96-well plates. The medium was removed after 24 h, and the cells were washed with PBS three times and fixed with 4% paraformaldehyde. Then, the cytoskeleton and nucleus were characterized and observed under a laser confocal microscope (Leica, Germany).

2.3. Preparation and characterization of hydrogels

2.3.1. Preparation of the porous Gel-Ca hydrogel

The porous Gel-Ca hydrogel was prepared by dissolving different concentrations of GelMA (8%, 12%, and 15%) into 0.1 M $CaCl_2$ solution containing 0.1% LAP photoinitiator. The solution was placed under a blue light at 405 nm for crosslinking. To obtain a hydrogel loaded with thrombin, the Gel-Ca hydrogel was freeze-dried to obtain a sponge scaffold, allowed to absorb the thrombin solution, and then freeze-dried again.

2.3.2. Preparation of HA hydrogel-loaded EVs

To prepare a HA hydrogel containing functional EVs and sVEGF, EVs were mixed in 8% HA solution containing 0.1% LAP initiator, and the hydrogel was prepared under 405 nm light irradiation with or without 3.75 mg/mL bevacizumab.

2.3.3. Scanning electron microscopy (SEM) and EDS analyses

The porous structures of the hydrogels were observed by SEM. Single- or double-layer hydrogels were freeze-dried and cut into pieces in the longitudinal direction. Each sample was sputter-coated with gold for 60 s and then directly visualized. Images were taken with a scanning electron microscope (Hitachi, S-4800). Moreover, the element distribution on the double-layer hydrogel was detected by EDS.

2.3.4. The effects of concentration on blood clotting

Different concentrations of thrombin were dropped into the freeze-dried Gel-Ca sponge scaffold until it was fully absorbed, and then the sponge was frozen again to obtain the Gel-Ca/Thr sponge scaffold loaded with thrombin. Fresh anticoagulated blood was treated with 0.1 M $CaCl_2$ at a 9:1 vol ratio and then added to the freeze-dried sponge to observe coagulation. After 1 min, the sponge was placed on filter paper, the blood was squeezed out, and blood coagulation was observed. After the optimal concentration of thrombin was identified, the treated blood was removed from the bottom of the Gel-Ca/Thr sponge scaffold to allow swelling and then photographed for observation.

2.3.5. Preparation of the lineage-specific multifunctional double-layer scaffold

To prepare a double-layer functional hydrogel with a stable and inseparable interface layer, GelMA at different concentrations was dissolved in 0.1 M $CaCl_2$ solution containing 0.1% LAP and gelatinized by irradiation with blue light. When the surface had a certain fluidity, the viscous HA solution was poured in, part of the solution was allowed to penetrate, and crosslinking was rapidly performed under blue light. Moreover, the two layers of the surface were exposed to blue light to fully react.

2.3.6. EV release analysis

For the release test, 200 μl of HA solution loaded with 1×10^{10}/mL EVs was added to the upper chamber of a 24-well Transwell plate for light crosslinking (0.4 μm to prevent the gel degradation products from affecting the test results). Then, 1 ml of PBS was added to the chamber, and 1 ml of PBS was added to the bottom of the plate. Then, the transwell plate was incubated at 37 °C. For testing, 10 μL of solution from the lower chamber was removed every 2 days, and the concentration of sEVs was measured by NTA.

2.4. Isolation and culture of BMSCs and chondrocytes

2.4.1. Isolation and culture of the cells

The femurs and tibias of 4-week-old SD rats were used to extract BMSCs and chondrocytes. For BMSCs extraction, after the SD rats were euthanized under excessive anaesthesia, the marrow cavity was washed under sterile conditions and placed in a 25 T culture flask for primary culture. The primary cells were grown in alpha-modified MEM (α-MEM; HyClone, USA) containing 15% foetal bovine serum (FBS, Gibco) and 1% penicillin/streptomycin (Gibco, USA) and incubated at 37 °C with 5% CO_2. When the cells reached 80% confluence, trypsin containing 0.25% EDTA was used for digestion and passage, and passage 2–3 cells were used for subsequent experiments.

For the extraction of rat or rabbit chondrocytes, the transparent cartilage layer on the cartilage surface was carefully scraped with a surgical blade and washed in a dish containing cold PBS. Then, the cartilage fragments were collected in a centrifuge tube, and pancreatin containing 0.25% EDTA was added for digestion for 0.5 h. The fragments were collected by centrifugation and digested in DMEM (high glucose) containing 0.2% type II collagenase for 8 h. The suspension was filtered through 100-μm nylon mesh filters to obtain the primary chondrocytes. The primary chondrocytes were cultured in DMEM containing 10% FBS at 37 °C with 5% CO_2. The medium was changed every three days. When the cells reached 80% confluence, they were passaged, and passage 2–3 cells were used for subsequent experiments.

2.4.2. Flow cytometry

A suspension of 1×10^6 BMSCs at passage 3 was stained with fluorescently labelled antibodies for marking and detection by flow cytometry. The following antibodies were used: CD45-APC (BioLegend), CD44-PB (BioLegend), and CD29-PE/Cy7 (BioLegend).

2.5. Biocompatibility and cytotoxicity assay

Cytotoxicity was evaluated using the Cell Counting Kit-8 (CCK-8) assay (Dojindo, Japan). BMSCs or chondrocytes were cultured at a density of 3000 cells per well in a 96-well plate in growth medium and incubated at 37 °C for 24 h in a humid atmosphere containing 5% CO_2 with different treatments. After 24 h, 48 h and 72 h, the cells were washed with PBS again, and 100 μl of CCK-8 solution was added to the cells for another 2 h. The absorbance of each well was measured at 450 nm with an enzyme marker (SpectraMax iD3, USA).

The activity and morphology of the cells were observed by live/dead staining. BMSCs and chondrocytes were cultured with different treatments at 37 °C under 5% CO_2 for 72 h. Subsequently, the sample solution was removed, and calcein-AM/propidium iodide (PI) (Bestbio, Shanghai, China) was added. After 30 min, the cells were washed with PBS three times. Finally, the dye was washed away, and PBS was added. Fluorescence images were observed under a confocal microscope at Ex/Em = 488/515 nm to observe AM, and Ex/Em = 561/617 nm to observe

PI.

2.6. Chondrocyte and differentiation assay

2.6.1. Quantitative RT–PCR analysis

Total RNA was extracted and purified from cells by using TRIzol reagent (TaKaRa), and cDNA was synthesized by reverse transcription of RNA (1200 ng) using the reverse first strand cDNA synthesis kit (Bio-Rad) [26]. The gene expression of Col 2, Acan, and Col 10 was determined and evaluated with a qPCR system (Bio-Rad) using a 20 μl reaction volume according to the manufacturer's instructions. The $2^{-\Delta\Delta CT}$ method was applied to calculate the fold change in gene expression [27]. GAPDH was used as a housekeeping gene. The primers are listed in Table S1.

2.6.2. Western blot analysis

Protein expression levels were detected by Western blotting as previously described [28]. Total protein was extracted and isolated from cell lysates with RIPA buffer, and the protein concentration was measured using a BCA protein assay kit. Equivalent amounts of proteins were separated by sodium dodecyl sulfate–polyacrylamide gel electrophoresis (SDS–PAGE) and transferred to 0.22 μm polyvinylidene difluoride (PVDF) membranes. The membranes were incubated with 5% BSA solution for blocking and then incubated with primary antibodies (CD81 (CST), Tsg 101 (CST), calnexin (CST), aggrecan (Agg, Abcam), GAPDH (CST), SOX 9 (Abcam), Col 2 (Abcam), and Col 10 (Abcam)) overnight at 4 °C. After washing, the membranes were incubated with horseradish peroxidase-conjugated secondary antibodies at room temperature for 1 h. The protein bands were visualized with enhanced chemiluminescence-based detection reagent (ECL, Tanon).

2.6.3. Pellet culture and histologic analysis

The effects of different treatment methods on cartilage formation were observed by coagulating stem cells for culture as previously described [29]. Briefly, each pellet consisted of 2.5×10^5 cells and was cultured in medium (DMEM +10% FBS +1% penicillin/streptomycin) for 2 weeks. The culture medium was supplemented or not with 3.75 mg/mL bevacizumab.

2.6.4. Alkaline phosphatase (ALP) staining and alizarin red staining

BMSCs (1×10^4) were seeded in a 24-well plate and cultured with or without the construct for 14 d. The medium was changed every 2 days. After 14 d, ALP staining was conducted by using the BCIP/NBT Alkaline Phosphatase (ALP) Color Development Kit (Beyotime, China), where deep blue represents positive expression. For ARS staining, the cells were fixed with 4% paraformaldehyde and then stained with alizarin red (Solarbio, China) for 3 h to observe calcium deposits.

2.7. mRNA-seq analysis

In brief, total RNA was extracted from rat chondrocytes seeded in 6-well plates using TRIzol. After extraction and sedimentation, RNA was dissolved in DEPC-treated water and quantified with a NanoDrop. After evaluation on an Agilent Technologies 2100 bioanalyzer, qualified samples were used to establish the final library. DNA nanoballs were loaded, and single-end 50-base reads were applied on the BGIseq 500 platform (BGI-Shenzhen, China).

2.8. In vivo evaluation using a rabbit osteochondral defect model

Animal experiments were reviewed and approved by the ethical review committee of Animal Research Committee of Shanghai Jiao Tong University General Hospital. Adult male New Zealand white rabbits weighing 3.0–3.5 kg were used for the in vivo study. Fifteen rabbits were randomized into five groups: control group without any treatment, HA@EV/Gel scaffold group, HA@EV/Gel-Thr scaffold group, HA@St-EV/Gel-Thr scaffold group and HA@St-EV + sVEGF/Gel-Thr scaffold group. After anaesthesia with ethyl carbamate (0.2 g/mL) through the ear vein, the knee joints of the rabbits were shaved and exposed using an anteromedial parapatellar incision. The osteochondral defect (5 mm in diameter, 4 mm in depth) was created using a corneal trephine on the trochlear groove of the distal femur. Then, double-layer scaffolds were implanted to match the defect. Eight weeks after the operation, the rabbits were sacrificed to harvest the knee joints. The International Cartilage Repair Society (ICRS) macroscopic evaluation scale was used for each group of samples and is shown in Table S2. MRI analysis was performed by a Siemens TIM Trio 2.0 T (T) MRI scanner (Siemens, Erlangen, Germany) and microcomputed tomography (μCT) scanning was carried out by a micro-CT system (SkyScan 1172, Bruker, Belgium). Sections (4 μm thick) in the centre of the operative site of the decalcified tissue samples were sliced using a tissue slicer and stained with H&E, Safranin O, fast green and alcian blue.

2.9. Statistical analysis

The data are expressed as the mean ± standard deviation (s.d.). The experiments were repeated at least three times. The groups were compared using one-way or two-way analysis of variance (ANOVA) followed by Tukey's post hoc test for multiple comparisons. A value of $P < 0.05$ was considered to indicate statistical significance.

3. Results and discussion

3.1. Extraction and identification of starved BMSCs-EVs

Starved BMSCs-EVs were collected by ultracentrifugation (Fig. 1A). EVs with a typical cup-shaped morphology were observed by TEM (Fig. 1B). The results of NTA showed that the diameter of the extracted EVs had a narrow distribution, and the average diameter was approximately 141 nm. The expression of the markers CD81, TSG and calnexin in starved BMSCs-EVs was detected by Western blotting, and starved BMSCs-EVs exhibited EV-specific surface markers such as CD81 and TSG101 but not calnexin. After incubating PKH26-labelled starved BMSCs-EVs with chondrocytes or BMSCs at a concentration of 1×10^9/mL for 12 h, confocal images were taken. The 2D image in Fig. 1E demonstrates the effective uptake of starved BMSCs-EVs by chondrocytes and BMSCs.

3.2. Preparation and characterization of the double-layer hydrogel

We next set out to prepare a porous hydrogel layer that can quickly absorb blood and form a haematoma to repair subchondral bone. First, to determine the appropriate concentration, GelMA-Ca hydrogels with polymer concentrations of 8%, 12% and 15% were prepared (Fig. 2A). The morphology of the hydrogel was observed by SEM (Fig. 2B). With increasing concentrations, the pores of the porous structure gradually became smaller. The HA layer containing starved BMSCs-EVs and the Gel-Ca layer with different concentrations were prepared into a double hydrogel layer (Fig. 2C). During the preparation of the double hydrogel layer, before crosslinking of the lower layer was complete, the viscous upper liquid was poured in for crosslinking. Due to partial penetration, the two layers bound tightly and did not separate. The bonding strength between the two layers was observed by SEM and forced bending experiments. The results showed that the two layers formed tight junctions that are difficult to separate (Fig. 2D and E). The element distribution of the double hydrogel was observed by EDS, and the amount of calcium in the Gel-Ga layer was significantly greater than that in the HA layer (Fig. 2E). Next, a double-layer gel containing thrombin was prepared. First, the appropriate concentration of thrombin was determined. Gel-Ca sponge layers with different concentrations of thrombin was prepared were absorption and freeze drying. The same amount of blood was absorbed into the sponge for 1 min, and the sponge was placed on dust-

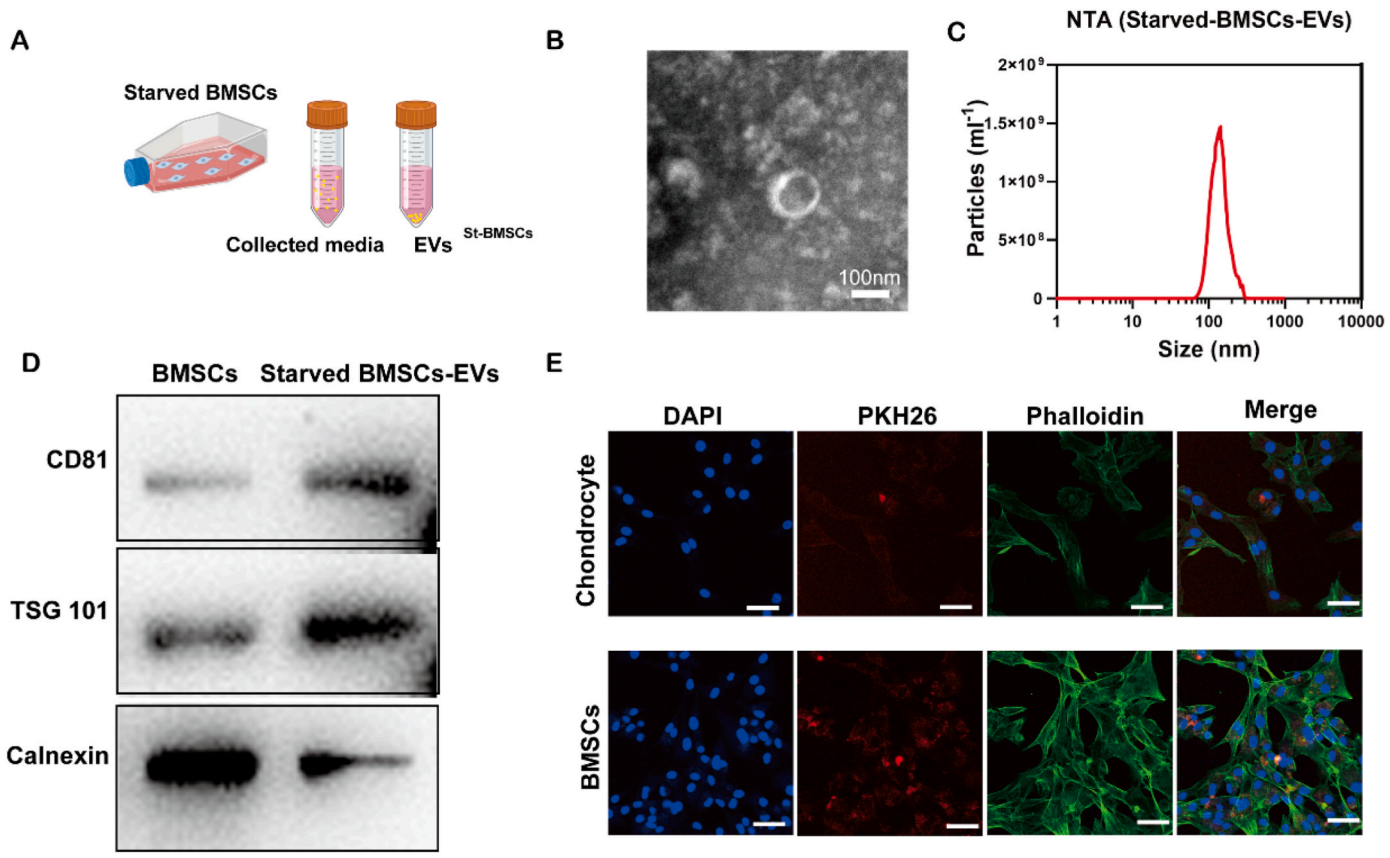

Fig. 1. Characterization of the starved BMSCs-Evs. A. Schematic illustration of the isolation of starved-BMSCs-Evs. B. TEM image of starved-BMSCs-Evs. C. The particle size distribution of starved-BMSCs-Evs measured by nanoparticle tracking analysis. D. Western blot analysis of sEV-specific surface markers. E. Chondrocyte and BMSCs uptake of PKH26-labelled starved BMSCs-Evs.

free paper to observe blood coagulation. Finally, a concentration of 0.5 mg/mL thrombin was selected to prepare the lower layer (Fig. 2F). Blood absorption and coagulation experiments were performed on double-layer scaffolds with different concentrations of Gel-Ca containing thrombin. The results demonstrated that after the same amount of blood was added from the bottom surface, the HA/8% Gel-Ca hydrogel with a macroporous structure could absorb blood quickly, but the blood invaded the cartilage layer during blood coagulation. As the pore size decreased, the blood coagulation interface gradually decreased, and the formed haematoma also decreased in size (Fig. 2G). Therefore, to absorb more blood to form a haematoma and prevent it from entering the cartilage layer, the HA/12% Gel-Ca double-layer gel was finally selected for subsequent experiments. Fig. 2H presents the hydrogel morphology before and after coagulation. The kinetic behaviour of gel release from starved BMSCs-EVs was tested by transwell assays (0.4 μm to prevent hydrogel degradation particles from affecting the test) and NTA. The results demonstrated slow release (Fig. 2I).

3.3. The HA hydrogel containing starved BMSCs-sEVs and sVEGF promoted the proliferation of chondrocytes

Hyaluronic acid (HA) is a natural extracellular matrix in tissues that is of great significance in biomaterial science and biomedical engineering [30,31]. Therefore, HA was used as the matrix material to promote cartilage differentiation and regeneration. Chondrocyte proliferation is required and important for cartilage regeneration via chondrocytes [32]. Previous reports have demonstrated that starved BMSCs-EVs significantly reduce chondrocyte apoptosis and promote proliferation and vitality [33]. Here, the results of the CCK-8 (Fig. 3A) and live/dead staining (Fig. 3B) assays demonstrate that the HA hydrogel loaded with starved BMSCs-EVs promotes the proliferation and vitality of BMSCs and chondrocytes.

3.4. The Gel-Ca/Thr hydrogel promoted the proliferation of BMSCs

BMSCs were identified by flow cytometry, and the results showed that these BMSCs highly expressed CD44 and CD29 (99.28%) but did not express CD45 (≤2%). High cell viability is necessary for ensuring successful differentiation and tissue regeneration [34]. The CCK8 assay and live/dead staining were used to evaluate the viability of the BMSCs cocultured with different GelMA-based hydrogels. As shown in Fig. 3C and D, compared with the control group, Gel-Thr slightly promoted the proliferation of stem cells; however, stem cells planted on the Gel-Ca gel exhibited more obvious promotion of proliferation. These results indicate that the gel layer used for promoting bone formation can promote the proliferation of bone marrow-derived stem cells, which is conducive to subsequent osteogenic differentiation. As previously reported, calcium-containing hydrogels can stimulate the proliferation of BMSCs and the differentiation of osteoblasts in vitro [35].

3.5. The HA hydrogel containing starved BMSCs-sEVs and sVEGF significantly enhanced chondrocyte function

When cartilage is damaged, it is difficult for chondrocytes adjacent to the cartilage defect to achieve self-healing due to impaired chondrocyte function and low chondrocyte vitality [36]. Therefore, enhancing the proliferation and biosynthetic processes of chondrocytes is crucial for the healing process. We investigated the effects of starved BMSC-EVs and sVEGF on the function of chondrocytes. The expression of genes and proteins related to cartilage differentiation and hypertrophy was

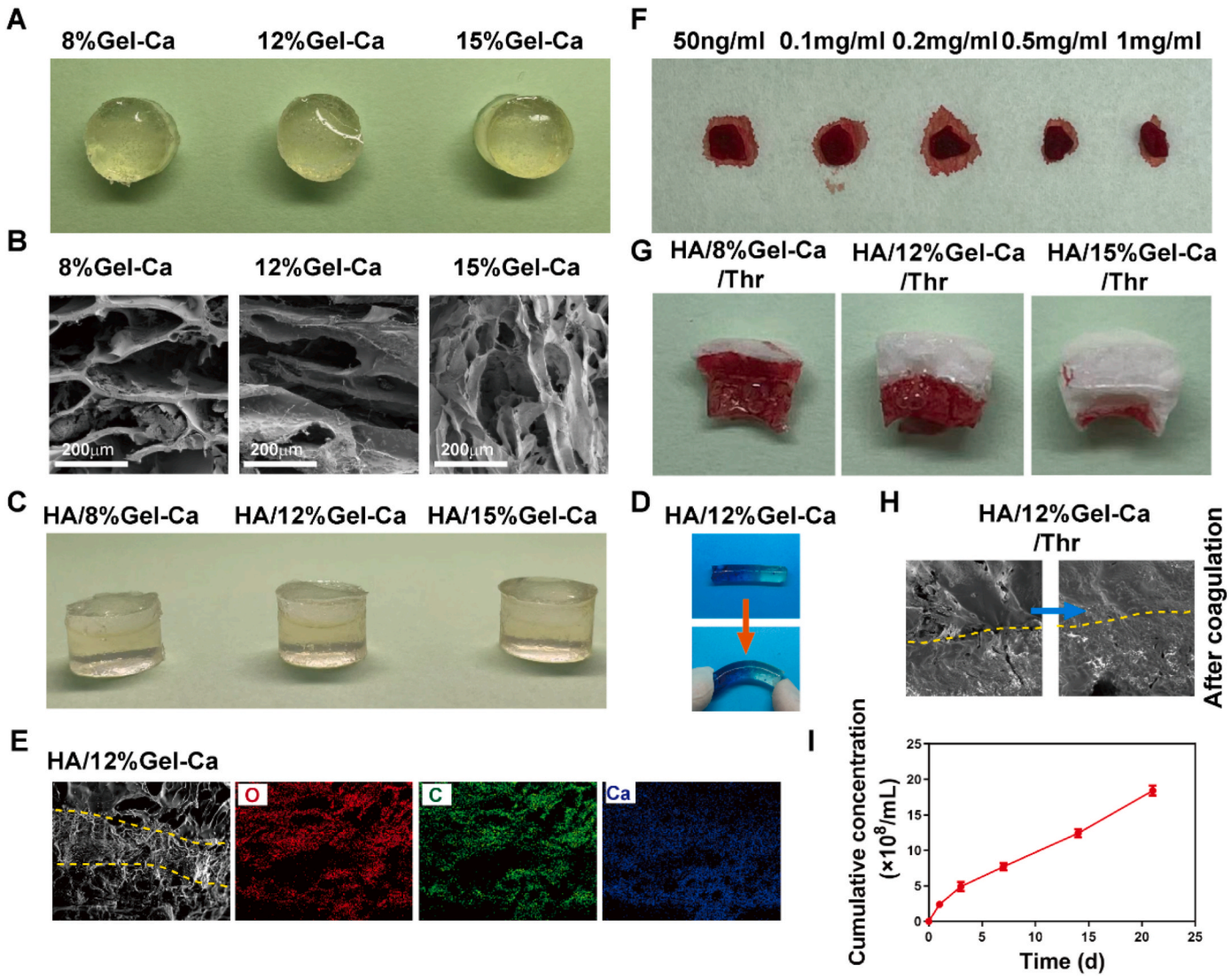

Fig. 2. Preparation and characterization of the cartilage and bone layer hydrogels. A. Gel-Ca hydrogels containing calcium salt and different polymer concentrations for repairing the subchondral bone layer. B. SEM images of the Gel-Ca hydrogels. C. Appearance of the double-layer hydrogels. D. The tight junction interface was still observed after the double-layer hydrogels were bent under force. E. EDS images of the HA/12% Gel-Ca double-layer hydrogel. F. Blood coagulation on Gel-Ca hydrogels with different concentrations of thrombin. G. Blood absorption and coagulation on the HA/Gel-Ca double-layer hydrogel. H. SEM images of the HA/12% Gel-Ca double-layer hydrogel before and after coagulation. I. Total release of starved BMSCs-EVs from the HA/12% Gel-Ca double-layer hydrogel after 21 days.

investigated by qPCR, WB and staining. On the 7th and 14th days, the HA hydrogel containing starved BMSC-EVs stimulated the upregulation of the cartilage-related genes Acan and Col 2, as shown in Fig. 4A and B. In addition, although Col 10 was upregulated on the 7th day after combination with sVEGF, the expression of Col 10 was significantly decreased on the 14th day, which demonstrated that the combination of starved BMSCs-EVs and sVEGF could promote cartilage differentiation and effectively prevent hypertrophy. Similarly, the expression of cartilage-associated proteins in chondrocytes after 14 days of coculture was examined. The HA hydrogel containing starved BMSCs-EVs upregulated the protein expression of aggrecan and Col 2 (Fig. 4 C, D), indicating that starved BMSCs-sEVs benefited the formation of glycosaminoglycan. After 21 days of 3D culture, the cells were examined (Fig. 4E). After sectioning the formed globules and observing the Alcian blue staining and collagen staining images, the microspheres treated with the HA hydrogel containing starved BMSCs-EVs expressed more GAG and Col 2. Moreover, the expression of Col 10 could be effectively reduced in the presence of sVEGF. Other studies have reported that the use of VEGF blockers and cartilage differentiation-inducing factors has a synergistically stronger ability to promote differentiation than the use of these factors alone while reducing the tendency of hypertrophy [37,38]. These results demonstrate that starved BMSC-EVs could significantly enhance chondrocyte function, including cartilage phenotype and cartilage formation, and the ability to form hyaline cartilage was synergistically improved with sVEGF.

To elucidate the underlying mechanism, we profiled mRNA expression in BMSCs-EVs and starved BMSCs-EVs through high-throughput mRNA sequencing. As shown in Fig. 5, there were 722 downregulated genes and 640 upregulated genes in chondrocytes treated with starved BMSCs-EVs compared to BMSCs-EVs (Fig. 5A). The top 20 KEGG pathways of the upregulated genes are listed in Fig. 5B. Among them, the foxo signalling pathway was found to be an important pathway related to regeneration. To further confirm the impact of the foxo pathway on the effects of starved BMSC-EVs, we analysed the expression of the foxo1 and foxo3a proteins. The results showed that treatment with starved BMSCs-EVs did indeed increase the expression of the foxo protein in chondrocytes (Fig. 5C) while simultaneously increasing the expression of the cartilage-related transcription factor SOX 9 (Fig. 5D). The FOXO inhibitor AS1842856 prevented the upregulation of SOX 9 (Fig. 5D).

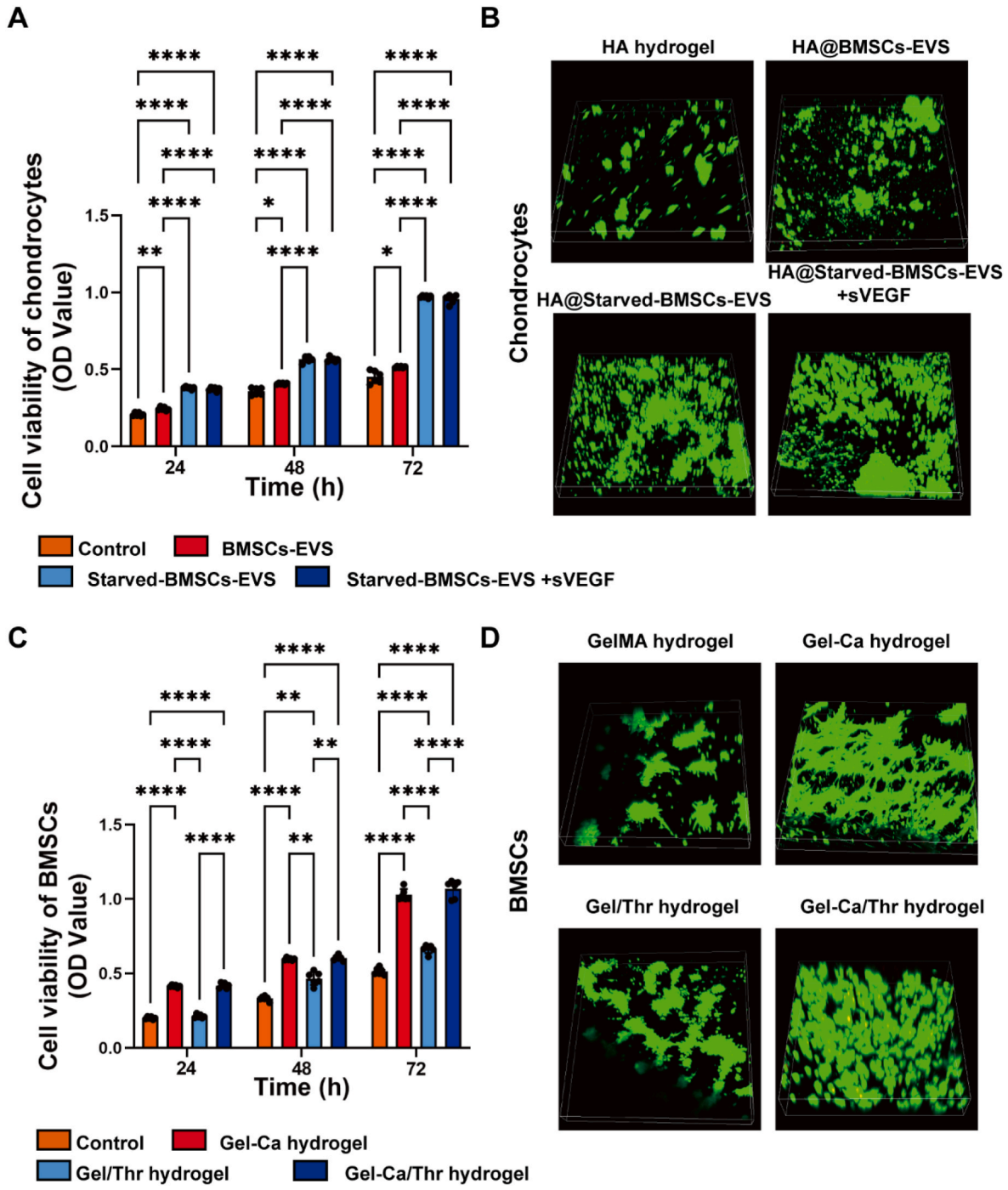

Fig. 3. Effect of starved BMSCs-sEVs and hydrogels on the viability of BMSCs and chondrocytes. A. CCK-8 values were measured in chondrocytes at 24, 48 and 72 h after coincubation. *P < 0.05, **P < 0.01, ****P < 0.0001. B. Live/dead staining of chondrocytes at 72 h after coincubation. C. CCK-8 values were measured in BMSCs at 24, 48 and 72 h after coincubation. **P < 0.01, ****P < 0.0001. D. Live/dead staining of BMSCs at 72 h after coincubation. Fluorescence staining with AM (green) representing live cells and PI (red) representing dead cells. (For interpretation of the references to color in this figure legend, the reader is referred to the Web version of this article.)

3.6. Lineage-specific multifunctional double-layer scaffold

ALP and Alizarin red staining showed that the lower layer distinctly promoted the expression of ALP and the formation of calcium nodules (Fig. 6A). The release of calcium ions promotes the osteogenic differentiation of BMSCs. To prepare a double-layer scaffold with the potential to differentiate, especially guided by the gel structure and bioactive factors, an HA-based solution with bioactive factors and a GelMA-based solution were prepared under sterile conditions and crosslinked successively. Transwell assays were used to culture the lineage-specific multifunctional scaffold and to observe region-specific differentiation (Fig. 6B). After 21 days of incubation, Col 2 and ALP expression were measured by PCR and immunofluorescence. The upper layer of HA@StEVs + sVEGF exhibited higher expression of extracellular matrix Col 2, whereas the lower layer Gel-Ca exhibited more obvious expression of extracellular matrix ALP. Together, these data demonstrate that this double layer could trigger the differentiation of BMSCs into chondrocytes and osteoblasts because the cells were in different culture

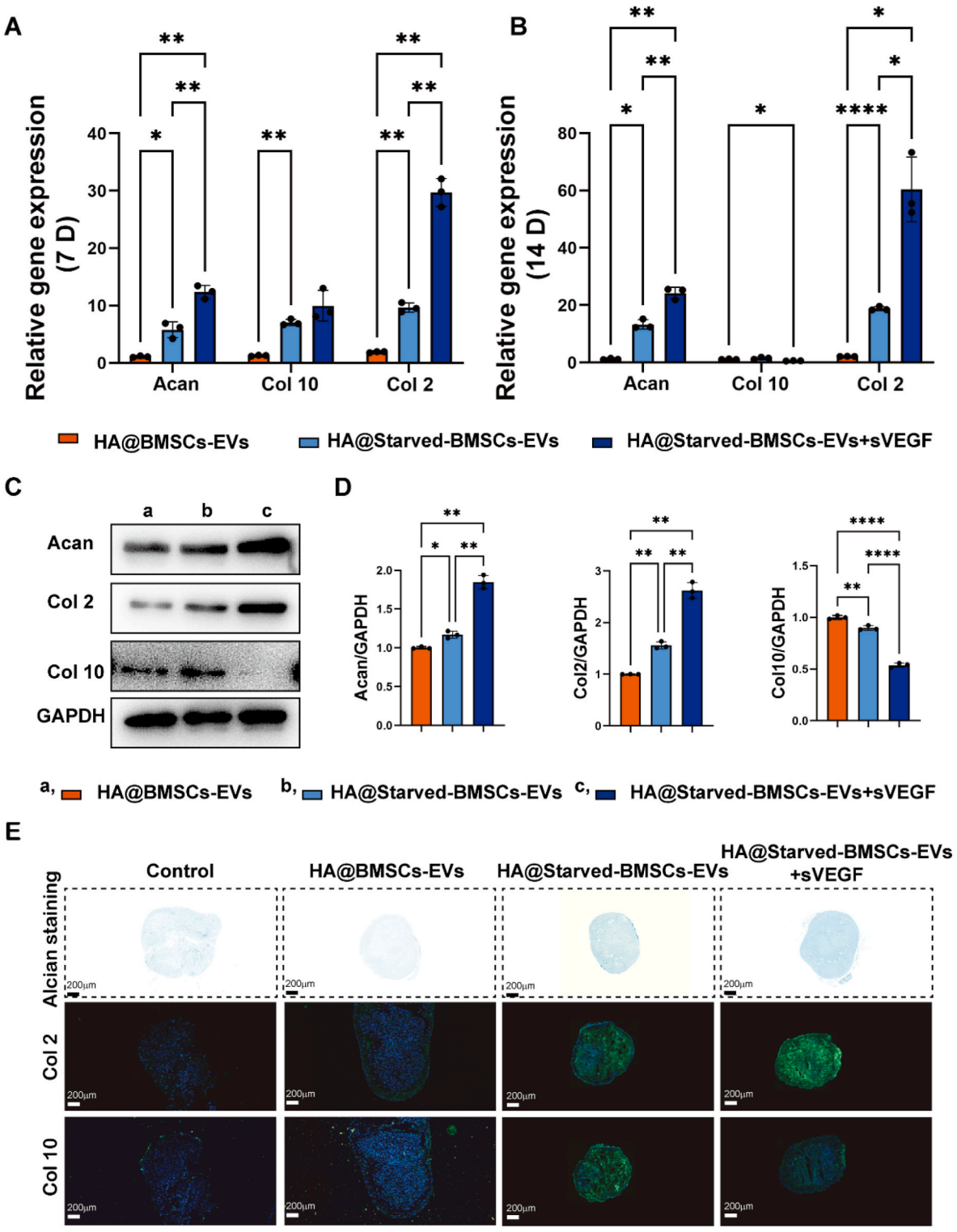

Fig. 4. Starved BMSCs-Evs enhanced the matrix synthesis of chondrocytes. Cartilage-related gene expression of aggrecan, Col2 and Col 10 was measured by qPCR, and the statistical results are presented. C-D. Cartilage-related protein expression tested by western blot and the statistical results. E. Alcian blue- and collagen-related staining of rBMSC microspheres. *P < 0.05, **P < 0.01, ****P < 0.0001. (For interpretation of the references to color in this figure legend, the reader is referred to the Web version of this article.)

microenvironments. Thus, the double-layer scaffold had good ability to promote lineage-specific induction (Fig. 5C–E).

3.7. In vivo evaluation of the integrated regeneration of cartilage and subchondral bone

New Zealand white rabbits were utilized in this study to investigate the regeneration of osteochondral tissues. Before the animal experiment, we investigated and confirmed the effect of starved BMSCs-EVs on the

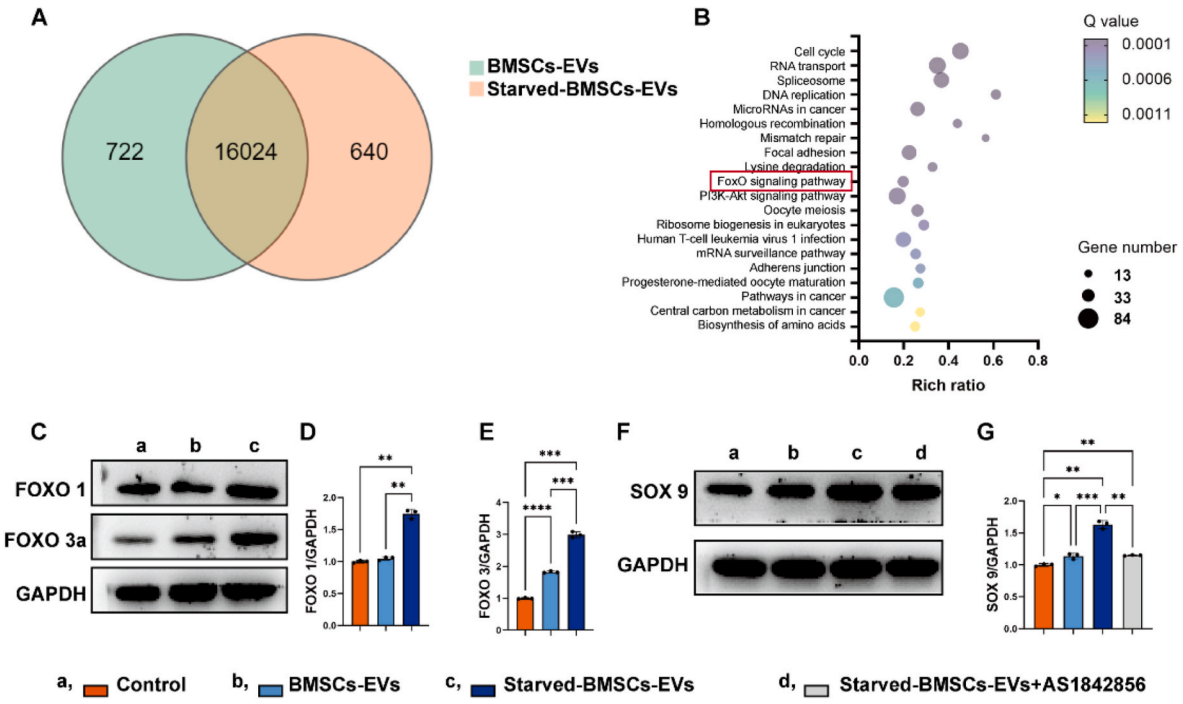

Fig. 5. RNA sequencing analysis. (A) Venn diagram of the overlapping differentially expressed genes between BMSCs-EVs and starved BMSCs-EVs ($q < 0.05$). (B) KEGG pathway analysis of the upregulated genes in chondrocytes treated with starved BMSCs-EVs. (C–E) Protein expression of foxo 1 and foxo 3a determined by Western blotting and analysed by ImageJ. (F–G) Protein expression of SOX 9 after different treatments (1 μM AS1842856 was used to inhibit the foxo pathway).

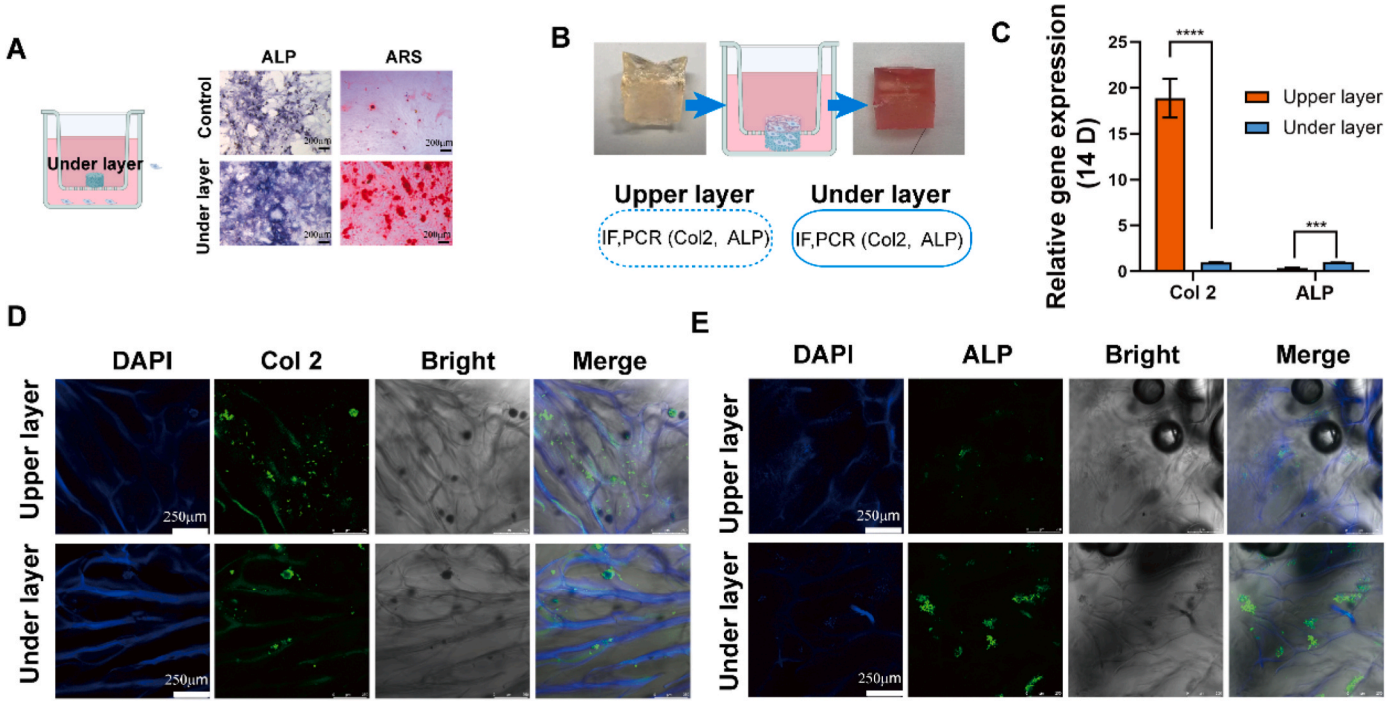

Fig. 6. The lineage-specific multifunctional scaffold induced zone-specific col 2 and alkaline phosphatase (ALP) expression, as determined by staining of each layer. A. The effect of the lower layer on the expression of ALP and calcium deposition (alizarin red staining) after 14 days of culture determined by transwell assays. B. Schematic illustration of the culture process with the bilayered constructs in the transwell assays. C. Differential expression of chondrogenesis- and osteogenesis-related genes induced in vitro after treatment with the bilayer constructs. D-E. Immunofluorescence staining of cartilage (col 2)- and bone (ALP)-related proteins. (For interpretation of the references to color in this figure legend, the reader is referred to the Web version of this article.)

proliferation and biosynthesis of rabbit chondrocytes (Fig. S2). An osteochondral defect in rabbit knees was established to evaluate cartilage and subchondral bone regeneration after implanting the lineage-specific multifunctional hydrogel. Gross observation of the defects in the distal femur was performed (Fig. 7A). In the control, HA@EVs/Gel, and HA@EVs/Gel-Thr groups, obvious defects could still be seen. However, defect repair in the HA@St-EVs/Gel-Thr group and HA@St-EVs + sVEGF/Gel-Thr group was greatly improved, particularly in the

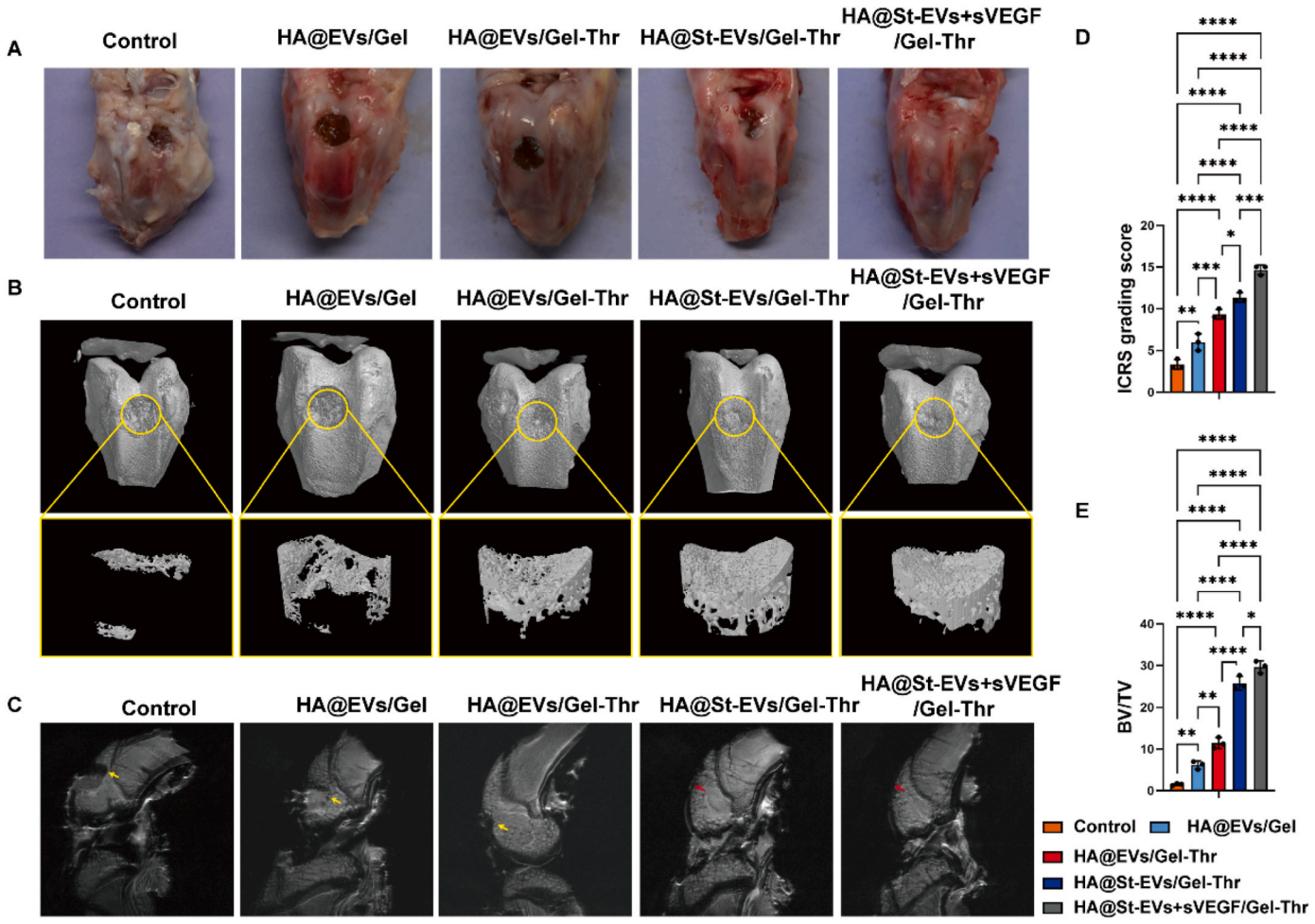

Fig. 7. In vivo evaluation of a lineage-specific multifunctional scaffold on integrated regeneration improvements in the rabbit model. (A) Gross images of the repaired osteochondral defects in each group at 8 weeks postsurgery. (B) micro-CT analysis of the repaired subchondral bone was conducted at 8 weeks in each group. (C) MRI imaging of repaired knees in each group at 8 weeks. The yellow arrow represents the defect. The red arrow represents new cartilage. (D)ICRS score grading of the cartilage defect. (n = 3. *p < 0.05, **p < 0.01, ***p < 0.001, ****p < 0.0001). (E) The volume ratio of the newly formed bone to defect regions. (n = 3. *p < 0.05, **p < 0.01, ****p < 0.0001). (For interpretation of the references to color in this figure legend, the reader is referred to the Web version of this article.)

HA@St-EVs + sVEGF/Gel-Thr group, in which the defects were almost completely repaired after 8 weeks (Fig. 7B). The average ICRS grading score in the HA@St-EVs + sVEGF/Gel-Thr group was significantly higher than that in the other groups at 8 weeks (Fig. 7D). Micro-CT imaging was then used to observe the formation of new bone 8 weeks after surgery. The control group exhibited less calcified tissue, which was only detectable at the edge of the defect area. The amount of calcified bone tissue in the HA@EVs/Gel group increased. Compared with these two groups, the three groups containing thrombin exhibited the formation of more calcified tissue, while the defects in the HA@St-EVs/Gel-Thr and HA@St-EVs + sVEGF/Gel-Thr groups exhibited the densest subchondral bone. In accordance with these observations, the HA@St-EVs + sVEGF/Gel-Thr group was undoubtedly associated with the highest bone volume/total volume (BV/TV) ratio (Fig. 7E). For further evaluation, the knee joint cartilage was examined by MRI. At 8 weeks after surgery, obvious defects were observed in both the control and HA@EVs/Gel groups. In contrast, in the HA@St-EVs/Gel-Thr group and HA@St-EVs + sVEGF/Gel-Thr group, full cartilage tissues were observed with surfaces that were more continuous and smoother than those in the control and HA@EVs/Gel groups (Fig. 7 C). Consistent with the gross observation, MRI and micro-CT results, HA@St-EVs + sVEGF/Gel-Thr was suitable to regenerate osteochondral defects. Repairing cartilage has always been a challenge in clinical osteochondral regeneration due to the low number and vitality of chondrocytes retained in the defect, especially in larger defects [39]. Therefore, some studies have tried to introduce chondrocytes into cartilage defects to induce cartilage regeneration. However, the need to expand a large number of cells in vitro requires considerable economic and time costs, and proliferating cells are prone to losing their ability to differentiate, which limits their application [40]. Therefore, this study has significant advantages in inducing and activating the vitality of chondrocytes in situ, promoting their proliferation and differentiation.

Finally, we observed the microstructure of the regenerated tissue by staining tissue sections and evaluated the ability of the lineage-specific multifunctional double-layer hydrogels to repair cartilage and subchondral bone in vivo (Fig. 8). In the untreated control group, the cartilage defect was covered by some regenerative tissue, but the regenerative tissue was disorderly arranged with abnormal staining different from the normal cartilage, and this group still exhibited obvious bone defects and cartilage defects. In the HA/Gel-Ca loaded with BMSC-EV group, the lower bone layer exhibited obvious defects, and no induced cartilage tissue was observed in the cartilage layer (weak alcian blue staining and safranin staining). After treatment with the double-layer hydrogel containing thrombin, although the cartilage layer did not regenerate significantly, the regeneration of the subchondral bone layer was significantly improved, which demonstrates that the regeneration of the lower bone layer could be accelerated by promoting blood coagulation and forming a haematoma. In the HA@St-EV/Gel-Thr

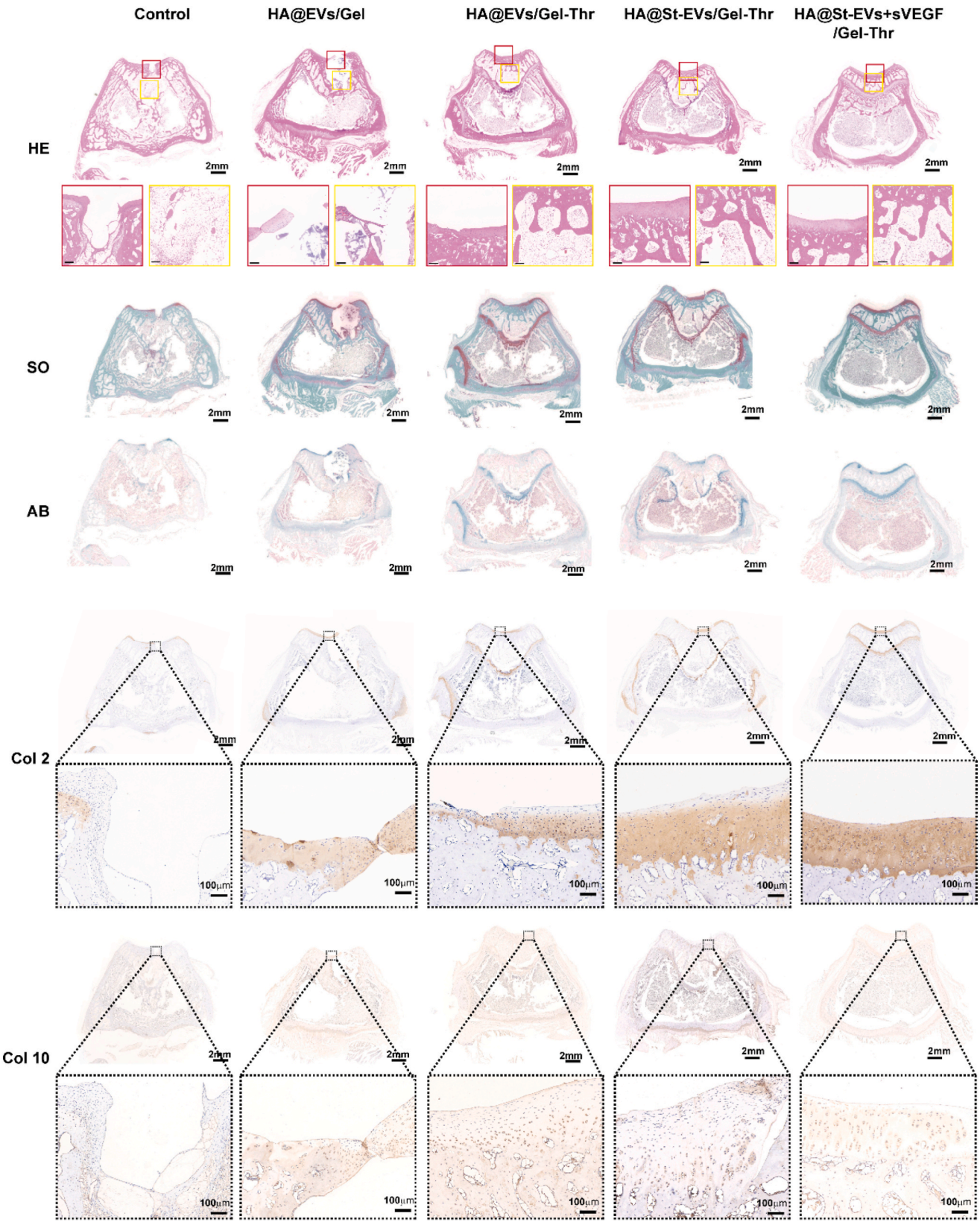

Fig. 8. Histological analysis of the regeneration of cartilage and subchondral bone tissues through HE staining, safranin-O and fast green staining and alcian blue staining, and immunochemistry for col 2 and col 10 expression. The lineage-specific multifunctional scaffold promoted the regeneration of osteochondral defects at 8 weeks. The red box represents the cartilage defect area, while the yellow box represents the subchondral bone defect area. (For interpretation of the references to color in this figure legend, the reader is referred to the Web version of this article.)

and HA@St-EV + sVEGF/Gel-Thr groups, the ability of the cartilage to regenerate was significantly improved, especially in the HA@St-EV + sVEGF/Gel-Thr group, as shown by Col 2 immunohistochemical staining. Furthermore, the Col 10 expression was lower in the HA@St-EV + sVEGF/Gel-Thr group than in the HA@St-EV/Gel-Thr group. Additionally, Col 2 was the predominant collagen in the regenerated cartilage in the HA@St-EV + sVEGF/Gel-Thr group, suggesting that the regenerated area mainly contained hyaline-like cartilage without fibrillation, which demonstrates that starved BMSC-sEVs and sVEGF could synergistically accelerate the regeneration of hyaline-like cartilage. By using a biomaterial-based antiangiogenic drug release system to block angiogenesis and combining it with functionalized exocrine secretion to provide activated chondrocyte activity, this system effectively enhanced chondrocyte function, promoted proliferation, metabolism, and extracellular matrix secretion, and provided a suitable environment for stable cartilage formation after implantation. These results demonstrate that the HA@St-EV + sVEGF/Gel-Thr lineage-specific multifunctional double-layer hydrogel can effectively promote the integrated regeneration of cartilage and inferior bone.

4. Conclusion

The integrated regeneration of cartilage and inferior bone is important for achieving not only structural recovery but also functional recovery of the whole joint. In this study, the combination of starvation-treated functional EVs and the angiogenesis inhibitor sVEGF significantly promoted the proliferation and biosynthesis of chondrocytes and reduced cartilage hypertrophy, which is of great significance during the formation of hyaline cartilage. Moreover, the pores of the hydrogel can be blocked by rapidly forming a haematoma in situ to prevent the blood in the marrow cavity from invading the cartilage layer and thus affecting the stability of subsequent cartilage. On the other hand, the haematoma can accelerate bone survival. Here, a double-layer multifunctional hydrogel that can repair both the cartilage layer and the lower bone layer was prepared. The HA@St-EV + sVEGF/Gel-Thr hydrogel exhibited superior repair of integrated cartilage and lower bone in vivo. In summary, these results demonstrate the promising application of this construct for fabrication into OC tissues with lineage-specific multifunctional double-layer scaffolds.

CRediT authorship contribution statement

Chunhui Ma: Conceptualization, Investigation, Methodology, Data curation, Writing – review & editing. **Tao Wang:** Data curation, Methodology, Writing – review & editing. **Xinmeng Jin:** Investigation, Validation, Writing – review & editing. **Wanglin Zhang:** Validation, Visualization. **Qi Lv:** Resources, Validation, Supervision.

Declaration of competing interest

The authors declare that they have no known competing financial interests or personal relationships that could have appeared to influence the work reported in this paper.

Data availability

Data will be made available on request.

Acknowledgements

This work was financially supported by Shanghai Natural Science Foundation (22ZR1450300, 22ZR1456600) and Independent original basic research project of Tongji University (22120210567).

Appendix A. Supplementary data

Supplementary data related to this article can be found at https://doi.org/10.1016/j.mtbio.2023.100800.

References

[1] C. Lesage, et al., Material-assisted strategies for osteochondral defect repair, Adv. Sci. 9 (2022), e2200050.
[2] X. Liu, et al., A biomimetic biphasic osteochondral scaffold with layer-specific release of stem cell differentiation inducers for the reconstruction of osteochondral defects, Adv. Healthcare Mater. (2020), e2000076.
[3] H. Zhang, et al., 3D Printing hydrogel scaffolds with Nanohydroxyapatite gradient to effectively repair osteochondral defects in rats, Adv. Funct. Mater. 31 (2020).
[4] L.J. Kang, et al., Self-assembled hyaluronic acid nanoparticles for osteoarthritis treatment, Biomaterials 275 (2021), 120967.
[5] C.B. Highley, G.D. Prestwich, J.A. Burdick, Recent advances in hyaluronic acid hydrogels for biomedical applications, Curr. Opin. Biotechnol. 40 (2016) 35–40.
[6] J.W. Nichol, et al., Cell-laden microengineered gelatin methacrylate hydrogels, Biomaterials 31 (2010) 5536–5544.
[7] H. Kim, et al., Hyaluronate and its derivatives for customized biomedical applications, Biomaterials 123 (2017) 155–171.
[8] M.A. Brennan, P. Layrolle, D.J. Mooney, Biomaterials functionalized with MSC secreted extracellular vesicles and soluble factors for tissue regeneration, Adv. Funct. Mater. 30 (2020).
[9] I.K. Herrmann, M.J.A. Wood, G. Fuhrmann, Extracellular vesicles as a next-generation drug delivery platform, Nat. Nanotechnol. 16 (2021) 748–759.
[10] J. Phan, et al., Engineering mesenchymal stem cells to improve their exosome efficacy and yield for cell-free therapy, J. Extracell. Vesicles 7 (2018), 1522236.
[11] C. Chen, F. Loe, A. Blocki, Y. Peng, M. Raghunath, Applying macromolecular crowding to enhance extracellular matrix deposition and its remodeling in vitro for tissue engineering and cell-based therapies, Adv. Drug Deliv. Rev. 63 (2011) 277–290.
[12] H.P. Bei, P.M. Hung, H.L. Yeung, S. Wang, X. Zhao, Bone-a-Petite: engineering Exosomes towards bone, osteochondral, and cartilage repair, Small 17 (2021), e2101741.
[13] P. Yuan, et al., Extracellular vesicles derived from starving BMSCs enhance survival of chondrocyte aggregates in grafts by attenuating chondrocyte apoptosis and enabling stable cartilage regeneration for craniofacial reconstruction, Acta Biomater. 140 (2022) 659–673.
[14] N. van Gastel, et al., Lipid availability determines fate of skeletal progenitor cells via SOX9, Nature 579 (2020) 111–117.
[15] M. Centola, et al., Scaffold-based delivery of a clinically relevant anti-angiogenic drug promotes the formation of in vivo stable cartilage, Tissue Eng Part A 19 (2013) 1960–1971.
[16] L. Claes, S. Recknagel, A. Ignatius, Fracture healing under healthy and inflammatory conditions, Nat. Rev. Rheumatol. 8 (2012) 133–143.
[17] Y. Yang, Y. Xiao, Biomaterials regulating bone hematoma for osteogenesis, Adv. Healthcare Mater. (2020), e2000726.
[18] Y. Li, et al., Collagen-based biomaterials for bone tissue engineering, Mater. Des. 210 (2021), 110049.
[19] P.J. Harwood, J.B. Newman, A.L.R. Michael, (ii) an update on fracture healing and non-union, Orthopaedics and Trauma 24 (2010) 9–23.
[20] B.F.L. Lai, Y. Zou, D.E. Brooks, J.N. Kizhakkedathu, The influence of poly-N-[(2,2-dimethyl-1,3-dioxolane)methyl]acrylamide on fibrin polymerization, cross-linking and clot structure, Biomaterials 31 (2010) 5749–5758.
[21] H.T. Shiu, P.C. Leung, C.H. Ko, The roles of cellular and molecular components of a hematoma at early stage of bone healing, Journal of Tissue Engineering and Regenerative Medicine 12 (2018) e1911–e1925.
[22] L. Xiao, et al., The interplay between hemostasis and immune response in biomaterial development for osteogenesis, Mater. Today 54 (2022) 202–224.
[23] Y. Huang, et al., Effects of Chitin Whiskers on Physical Properties and osteoblast culture of alginate based Nanocomposite hydrogels, Biomacromolecules 16 (2015) 3499–3507.
[24] Y. Wu, et al., Core–shell structured porous calcium phosphate bioceramic spheres for enhanced bone regeneration, ACS Appl. Mater. Interfaces 14 (2022) 47491–47506.
[25] J. Yan, et al., Injectable alginate/hydroxyapatite gel scaffold combined with gelatin microspheres for drug delivery and bone tissue engineering, Mater. Sci. Eng. C 63 (2016) 274–284.
[26] W. Shi, et al., Structurally and functionally optimized silk-Fibroin-gelatin scaffold using 3D Printing to repair cartilage injury in vitro and in vivo, Adv. Mater. 29 (2017).
[27] K.J. Livak, T.D. Schmittgen, Analysis of relative gene expression data using real-time Quantitative PCR and the $2^{-\Delta\Delta CT}$ method, Methods 25 (2001) 402–408.
[28] Z. Qiao, et al., Bioinspired stratified electrowritten fiber-reinforced hydrogel constructs with layer-specific induction capacity for functional osteochondral regeneration, Biomaterials 266 (2021), 120385.
[29] C. Studle, et al., Spatially confined induction of endochondral ossification by functionalized hydrogels for ectopic engineering of osteochondral tissues, Biomaterials 171 (2018) 219–229.
[30] F. Ghorbani, et al., Photo-cross-linkable hyaluronic acid bioinks for bone and cartilage tissue engineering applications, Int. Mater. Rev. (2023) 1–42.

[31] C. Antich, et al., Bio-inspired hydrogel composed of hyaluronic acid and alginate as a potential bioink for 3D bioprinting of articular cartilage engineering constructs, Acta Biomater. 106 (2020) 114–123.
[32] Q. Shen, et al., Fabrication of chondroitin sulfate calcium complex and its chondrocyte proliferation in vitro, Carbohydr. Polym. 254 (2021), 117282.
[33] Y. Kuang, et al., Adipose-derived mesenchymal stem cells reduce autophagy in stroke mice by extracellular vesicle transfer of miR-25, J. Extracell. Vesicles 10 (2020), e12024.
[34] W. Dai, et al., 3D bioprinting of heterogeneous constructs providing tissue-specific microenvironment based on host–guest modulated dynamic hydrogel bioink for osteochondral regeneration, Adv. Funct. Mater. 32 (2022).
[35] P. Diaz-Rodriguez, P. Garcia-Triñanes, M.M. Echezarreta López, A. Santoveña, M. Landin, Mineralized alginate hydrogels using marine carbonates for bone tissue engineering applications, Carbohydr. Polym. 195 (2018) 235–242.
[36] S. Stegen, et al., De novo serine synthesis regulates chondrocyte proliferation during bone development and repair, Bone Research 10 (2022) 14.
[37] T. Matsumoto, et al., Cartilage repair in a rat model of osteoarthritis through intraarticular transplantation of muscle-derived stem cells expressing bone morphogenetic protein 4 and soluble flt-1, Arthritis Rheum. 60 (2009) 1390–1405.
[38] S. Kubo, et al., 9.5 Blocking VEGF with sFlti improves the chondrogenic regeneration capacity of skeletal muscle-derived stem cells, Osteoarthritis Cartilage 15 (2007).
[39] T.Z. Li, et al., Using cartilage extracellular matrix (CECM) membrane to enhance the reparability of the bone marrow stimulation technique for articular cartilage defect in canine model, Adv. Funct. Mater. 22 (2012) 4292–4300.
[40] C. Vinatier, D. Mrugala, C. Jorgensen, J. Guicheux, D. Noël, Cartilage engineering: a crucial combination of cells, biomaterials and biofactors, Trends Biotechnol. 27 (2009) 307–314.